

Light-Induced Quantum Droplet Phases of Lattice Bosons in Multimode Cavities

P. Karpov^{1,2,3,4,*} and F. Piazza^{1,†}

¹Max Planck Institute for the Physics of Complex Systems, Nöthnitzer Straße 38, Dresden 01187, Germany

²Arnold Sommerfeld Center for Theoretical Physics, Ludwig Maximilian University of Munich, Theresienstr. 37, Munich 80333, Germany

³Munich Center for Quantum Science and Technology (MCQST), Schellingstr. 4, Munich 80799, Germany

⁴National University of Science and Technology “MISIS”, Moscow 119991, Russia



(Received 29 June 2021; accepted 7 February 2022; published 11 March 2022)

Multimode optical cavities can be used to implement interatomic interactions which are highly tunable in strength and range. For bosonic atoms trapped in an optical lattice we show that, for any finite range of the cavity-mediated interaction, quantum self-bound droplets dominate the ground state phase diagram. Their size and in turn density is not externally fixed but rather emerges from the competition between local repulsion and finite-range cavity-mediated attraction. We identify two different regimes of the phase diagram. In the strongly glued regime, the interaction range exceeds the droplet size and the physics resembles the one of the standard Bose-Hubbard model in a (self-consistent) external potential, where in the phase diagram two incompressible droplet phases with different filling are separated by one with a superfluid core. In the opposite weakly glued regime, we find instead direct first order transitions between the two incompressible phases, as well as pronounced metastability. The cavity field leaking out of the mirrors can be measured to distinguish between the various types of droplets.

DOI: [10.1103/PhysRevLett.128.103201](https://doi.org/10.1103/PhysRevLett.128.103201)

Introduction.—Ultracold atoms in optical cavities represent a unique experimental platform for the study of strongly interacting quantum many-body systems of light and matter [1,2]. Recent experiments involving a single-mode cavity [3,4] have implemented a Bose-Hubbard (BH) model extended by a global-range cavity-mediated interaction [5–15]. A rich phase diagram has been observed, featuring, besides the known compressible superfluid and incompressible Mott-insulating phases, a lattice supersolid as well as an incompressible density-wave phase.

The use of a second cavity mode has allowed us to observe a supersolid with continuous translational symmetry breaking [16–19]. By tuning cavities around the confocal degenerate point [20,21], it has become possible to even control the range of the cavity-mediated interaction [22,23], and to realize an optical lattice featuring phonons [24]. With finite-range cavity-mediated interactions, supersolids have been predicted to feature crystalline topological defects and to appear through non-mean-field phase transition dominated by fluctuations [25,26].

Here, we study a BH model extended by an attractive tunable-range interaction which can be realized in

state-of-the-art confocal-cavity experiments. We demonstrate that, due to the competition between cavity-mediated finite-range attraction and the on-site repulsion, the phase diagram is actually dominated by a variety of phases of droplets, i.e., self-bound many-particle quantum objects. These feature one or multiple compressible or incompressible shells, and for sign-changing interactions can become supersolid or density-wave modulated. Extended phases exist instead only for sufficient repulsion (see [27] for the classical, purely attractive case). We identify two physically different regimes. When the attractive interaction range exceeds the size of the droplet, the latter is strongly glued and its phase diagram can be qualitatively explained via the standard BH model in a self-consistent trap determined by the long-range interaction potential. Here, two incompressible droplet phases of different fillings are separated by one with a superfluid core. In the opposite weakly glued regime, we find a direct first-order transition between the two incompressible droplets. This is due to the strong dependence of the energy on the droplet density profile in this locally interacting regime, which also results in pronounced metastability. The light leaking out of the cavity offers a nondestructive experimental probe to distinguish between the different droplet phases, as the coherent part contains information about the density profile while the incoherent one encodes the density correlations. We compute the ground-state phase diagram with a worm quantum Monte Carlo (QMC) algorithm, using a canonical version [28–30] necessary to describe droplet phases.

Published by the American Physical Society under the terms of the [Creative Commons Attribution 4.0 International](https://creativecommons.org/licenses/by/4.0/) license. Further distribution of this work must maintain attribution to the author(s) and the published article's title, journal citation, and DOI. Open access publication funded by the Max Planck Society.

Without the lattice, quantum droplets of bosons have been experimentally observed using dipolar interactions [31–33] and bosonic mixtures [34,35], see [36] for review. In dipolar systems the anisotropic interactions lead to quantum-coherent (supersolid) chains of droplets [37–40], as well as other droplet arrangements [41–44] stabilized by long-range repulsion. Lattice bosons with dipolar interactions [45–48] and mixtures [49,50] have been proposed for implementing various types of extended Hubbard models [51]. While currently for dipolar gases and bosonic mixtures the challenge is to reach appreciable interactions beyond the nearest neighbor, cavity-mediated interactions are instead naturally strong at large distances. This feature is shared by other types of photon-mediated interactions based on refraction [52] or diffraction [53–55] (the latter also predicted to induce droplet phases [56,57]), which, however, lack the tunability of the range.

Model.—We consider ultracold bosons trapped in an optical lattice within a cavity. The system can be described by an extended BH model (see [58] for the derivation)

$$H = -t \sum_{\langle \mathbf{i}, \mathbf{j} \rangle} (\hat{b}_{\mathbf{i}}^{\dagger} \hat{b}_{\mathbf{j}} + \text{H.c.}) + \frac{U}{2} \sum_{\mathbf{i}} \hat{n}_{\mathbf{i}} (\hat{n}_{\mathbf{i}} - 1) + \sum_{\mathbf{i}, \mathbf{j}} V_{\mathbf{i}, \mathbf{j}} \hat{n}_{\mathbf{i}} \hat{n}_{\mathbf{j}}. \quad (1)$$

Here, $\langle \mathbf{i}, \mathbf{j} \rangle$ denotes nearest-neighbor sites in a D dimensional square lattice, with the linear size L t is the hopping between the nearest neighboring sites, $\hat{b}_{\mathbf{i}}^{\dagger}$ and $\hat{b}_{\mathbf{i}}$ are bosonic creation and annihilation operators, $\hat{n}_{\mathbf{i}} = \hat{b}_{\mathbf{i}}^{\dagger} \hat{b}_{\mathbf{i}}$, $U > 0$ is the on-site contact repulsion, and $V_{\mathbf{i}, \mathbf{j}}$ is the tunable-range cavity-mediated interaction between particles at sites \mathbf{i} and \mathbf{j} . In the main text we consider the quasi-1D geometry illustrated in Fig. 1, and in the Supplemental Material [58] a quasi-2D geometry is considered. In a multimode optical cavity, the finite range ξ is achieved by having a large number of transverse modes within a given degenerate family. Alternatively, Floquet modulation [59] or multifrequency driving [60] can render the range finite even for nondegenerate cavities. Experiments with ultracold bosons in confocal cavities have demonstrated the ability to tune this range [22]. We model this using the following generic form of the interaction potential:

$$V_{\mathbf{i}, \mathbf{j}} \equiv V_{\mathbf{i}-\mathbf{j}} = -V_0 \exp\left(-\frac{|\mathbf{i}-\mathbf{j}|^2}{\xi^2}\right), \quad (2)$$

where $V_0 > 0$ (attractive interaction). All lengths are measured in the unit of lattice spacing. We stress that the results presented in the following do not qualitatively depend on the particular form of interaction, as long as a single scale ξ can be associated with it. The latter helps to define a proper thermodynamic limit for a droplet phase, given by $L \rightarrow \infty$, $N \rightarrow \infty$, $\xi \rightarrow \infty$, $V_0 \rightarrow 0$, while $V_0 \xi^D = \text{const}$ and $N/\xi^D = \text{const} \simeq n_0$. Here, $V_0 \xi^D$ gives the

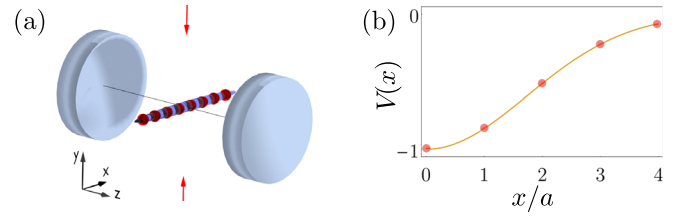


FIG. 1. (a) A quasi-1D gas is trapped in an optical lattice within the midplane of the cavity $z = 0$, along the x direction. The interactions are generated in the dispersive regime via two-photon transitions involving retroreflected laser beams (red arrows) which are red detuned from a given degenerate family of a multimode cavity. The interaction potential results from the interference between the laser and the cavity field. The trapping optical-lattice potentials are generated by three additional far-off detuned lasers (oriented along the x , y , and z directions, not shown) which do not interfere with the cavity field [4]. (b) Cavity-induced interaction, which decays over a scale ξ controlled by the number of degenerate, transverse cavity modes [22,61].

characteristic integrated interaction strength and the “droplet filling” n_0 gives the characteristic density of particles in a droplet of radius ξ . A further important parameter is the characteristic slope of the density profile, $\sigma \simeq \max(dn/dr) \simeq n_0/\xi = N/\xi^{D+1}$ (see [58]). This “steepness” parameter vanishes in the droplet thermodynamic limit defined above, and quantifies the amount of finite-size effects in the phase diagram. As we discuss later and in [58], these finite-size effects are experimentally measurable and have to be considered for the correct extrapolation to the thermodynamic limit.

Method.—We map the ground-state phase diagram of the model using a canonical worm QMC algorithm [28–30] with a fixed total number of particles $N = \sum_{\mathbf{i}} n_{\mathbf{i}}$ and periodic boundary conditions. Since we explicitly work in the canonical ensemble, we can deal with arbitrary occupation numbers (up to the total number of particles in the system). For the search of potential droplet phases the method is thus superior to other traditional methods of studying the BH model, like grand-canonical QMC [62–64] methods or density matrix renormalization group [65], which require fine tuning of the chemical potential and/or moderate cutoffs for the local occupation. In order to construct the ground-state phase diagram of the model, we perform calculations at small nonzero temperature $T = 0.1t$ (and check that it is low enough by benchmarking versus Lanczos exact diagonalization in 1D for sizes up to $L = N = 16$ [58]).

We characterize the droplets using two observables. (i) The droplet order parameter $O_{\text{dr}} = (1/N) \times \sqrt{[N_s/(N_s - 1)] \sum_{\mathbf{i}} [n_{\mathbf{i}} - (N/N_s)]^2}$ where $N_s = L^D$. It characterizes the deviation from a uniform density $n_{\mathbf{i}} = N/N_s$ and is similar to the inverse participation ratio in real space. The normalization is chosen in such a way that for a single-site droplet $n_{\mathbf{i}} = N\delta_{\mathbf{i},0}$ we have $O_{\text{dr}} = 1$, while for the uniform density $O_{\text{dr}} = 0$. (ii) The single-particle

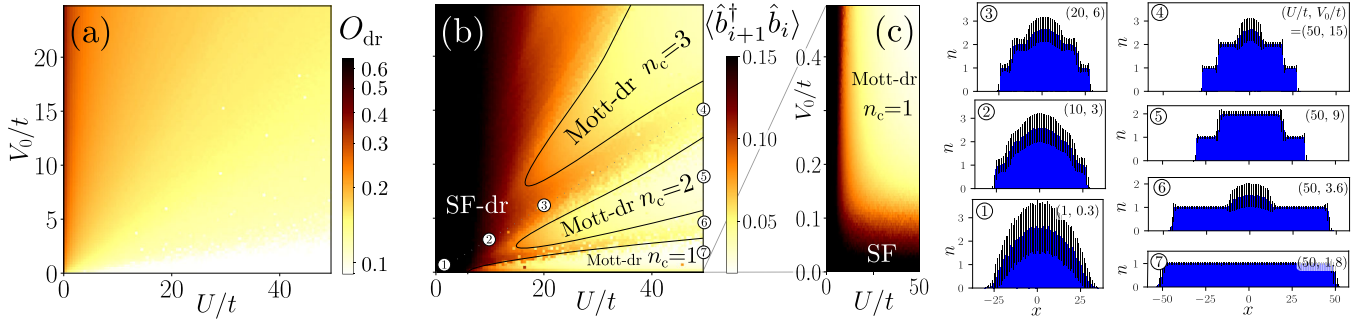


FIG. 2. The ground-state phase diagram in the coordinates V_0 (long-range attraction) vs U (on-site repulsion). The droplet thermodynamic limit ξ , $N \rightarrow \infty$ with $n_0 = N/\xi = 1$ is calculated by extrapolation up to $L = 500$, $N = 100$, $\xi = 100$. (a) Droplet order parameter O_{dr} . (b),(c) Nearest-neighbor superfluid correlator $\langle \hat{b}_{i+1}^\dagger \hat{b}_i \rangle$. Solid lines are guides for the eye indicating the crossovers between SF droplets and Mott droplets. (c) Close-up view into region $V_0/t < 0.5$ of (b), featuring the SF phase. Insets ①–⑦ show the spatial density profiles of the droplets at the corresponding points in the phase diagram; the error bars show the standard deviation of density from its mean value.

superfluid correlations between neighboring sites $\langle \hat{b}_{i+1}^\dagger \hat{b}_i \rangle$, used to distinguish superfluid from Mott phases.

Phase diagram.—Figure 2 shows the ground-state phase diagram. For $U = V_0 = 0$ the system is in the SF state. For $V_0 = 0$ and a fixed integer average filling $n = N/L$, upon increasing U we have a conventional SF-Mott transition at $U/t \approx 4n$ [66]. By increasing V_0 at $U = 0$ we enter a single-site droplet phase at $V_0/t \sim 1/N$ [67]. Upon increasing U and decreasing V_0 we observe smooth crossovers between droplets of different “diameters” [Fig. 2(a)] up to $d_{\text{max}} \simeq \min(L/2, N)$, bounded either by the size of the system or the total number of particles. After the maximum droplet size is reached, a first-order transition to a phase with uniform density occurs, either a Mott insulator for integer fillings or a SF for noninteger fillings. Figure 2(c) presents a close-up view into the $V_0/t < 0.5$ part of the phase diagram, featuring the extended SF phase. We can estimate the critical value of V_0 for the transition between the Mott droplet with the filling at the core $n_c = 1$ and the SF phase by equating the characteristic droplet energy $E_{\text{Mott-dr}} \sim -NV_0 \xi^D$ with the superfluid energy $E_{\text{SF}} \sim -Nt$, leading to $V_0 \sim t/\xi^D$.

Figure 2(b) shows the nearest-neighbor superfluid correlators, where we observe the various superfluid and Mott quantum droplet phases. The incompressible Mott phases correspond to different fillings at the core of the droplet, e.g., $n_c = 1, 2, 3$. The real-space density profiles of the droplet are shown as insets labeled by ①–⑦. Moving outward in the radial direction of the phase diagram we first observe the fully superfluid droplet ① (see [58] for an analytic Thomas-Fermi description), which gradually develops incompressible outer shells, and finally crossovers to a droplet with only the core being a compressible superfluid ④. Moving along a vertical line $U/t = 50$, the droplet core instead alternates between being compressible ④, ⑥ and incompressible ⑤, ⑦, while the outer shells remain incompressible. The succession of SF and Mott droplets

can be qualitatively understood using the standard BH phase diagram [68] in a trap, whereby the chemical potential is set by the local occupation at the droplet core. We emphasize, however, that, unlike the Mott-SF transitions in a trap, here the droplet size and density distribution are not externally fixed but rather emerge from the competition between local repulsion and finite-range attraction, since the droplet creates its own self-consistent trap by spontaneously breaking the translation symmetry of the Hamiltonian. In this situation, the superfluid core can be locally nucleated on top of an incompressible background, which results into smooth crossovers between SF and Mott droplets [see also Fig. 3(a)]. In contrast to the SF droplets, droplets containing one or more Mott shells become not only self-bound but also self-pinned, i.e., they do not move under the action of infinitesimal force. This is due to the fact that such movement occurs only as a perturbative process in t/U with the perturbation theory order growing with the size of Mott shells.

We explicitly checked (finite-size scaling data up to $L = 500$, $N = 100$, $\xi = 100$ presented in [58]) that the droplet regime of the phase diagram has a well-defined thermodynamic limit, $L, N, \xi \rightarrow \infty$, while $N/\xi = \text{const}$. For finite-size droplets featuring a steepness parameter $\sigma \gtrsim 1$, we observe additional features, e.g., mesoscopic first-order phase transitions associated with change in the droplet size [58].

Strongly and weakly glued droplets.—In the case considered so far in Fig. 2, the interaction range ξ was such that, even for the droplet of the maximum size d_{max} (i.e., the Mott droplet with $n_c = 1$), all the particles within the droplet interacted with each other. We call this the “strongly glued” regime $\xi \gtrsim d$. In the opposite regime of a “weakly glued” droplet $\xi \ll d$, each particle interacts only with $\sim N(\xi/d)^D$ neighboring particles.

Figures 3(a) and 3(f) compare the regimes of strongly and weakly glued droplets showing the $\langle \hat{b}_{i+1}^\dagger \hat{b}_i \rangle$ correlators

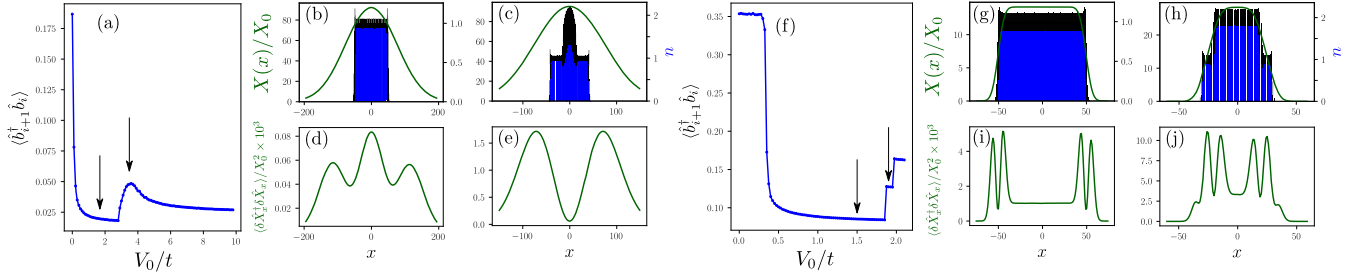


FIG. 3. Comparison between strongly and weakly glued droplets regimes. (a)–(e) Strongly glued droplet for $L = 500$, $N = 100$, $\xi = 100$, $U/t = 50$. (f)–(j) Weakly glued droplet for $L = 200$, $N = 100$, $\xi = 8$, $U/t = 25$. (a),(f) Nearest-neighbor superfluid correlators $\langle \hat{b}_{i+1}^\dagger \hat{b}_i \rangle$. Arrows indicate the values of V_0/t used in the neighboring panels. (b),(c),(g),(h) Dimensionless coherent cavity output $X(x)/X_0$ (where $X_0 = \Delta_a V_0 / g_0 \Omega_0$) and local particle density n . (d),(e),(i),(j) Dimensionless incoherent cavity output $\langle \delta \hat{X}_x^\dagger \delta \hat{X}_x \rangle / X_0^2$, where $\delta \hat{X}_x = \hat{X}_x - X(x)$. (b),(d) Mott droplet, $n_c = 1$, $V_0/t = 1.8$ (⊙ in Fig. 2). (c),(e) SF-droplet $V_0/t = 3.6$ (⊙ in Fig. 2). (g),(i) Mott droplet, $n_c = 1$, $V_0/t = 1.5$. (h),(j) Mott droplet $n_c = 2$, $V_0/t = 1.92$.

as a function of V_0 for a fixed value of U . In the strongly glued regime [Fig. 3(a)], the all-to-all character of interactions makes the interaction energy only weakly dependent on the density profile, which allows the SF core to continuously grow inside the Mott $n_c = 1$ bulk with increasing V_0 . As noted above, this regime can be understood as a BH model in an effective self-consistent trap. On the other hand, in the weakly glued regime [Fig. 3(f)], we observe instead a direct first-order phase transition between the $n_c = 1$ and $n_c = 2$ Mott droplets, without a SF component being nucleated. The transition corresponds to a sudden rearrangement of the density distribution in the bulk. This is preferred in this locally interacting regime: $\xi \ll d$, where the energy strongly depends on local changes of the density. This dependence introduces also a pronounced metastability, which renders QMC computations very demanding for large system's sizes.

Droplet imaging via the cavity.—The droplets can be nondestructively imaged using the cavity output. In the confocal-cavity experiments of [22,23] the inverse photon loss rate $1/\kappa$ is by far the fastest timescale. In this adiabatic regime the cavity field instantaneously adapts to the density of the atoms, so that photon correlators are proportional to density correlators. In particular, we get simple relations between the average density and the coherent component of the cavity field quadrature [58]:

$$X_{\mathbf{r}} \equiv \langle \hat{X}_{\mathbf{r}} \rangle \equiv \frac{1}{2} (\hat{a}_{\mathbf{r}} + \hat{a}_{\mathbf{r}}^\dagger) = -\frac{\Delta_a}{g_0 \Omega_0} \sum_{\mathbf{i}} V_{\mathbf{r},\mathbf{i}} \langle \hat{n}_{\mathbf{i}} \rangle, \quad (3)$$

where $\hat{a}_{\mathbf{r}}^\dagger$ is the creation operator for the cavity photon at position \mathbf{r} , $\Delta_a = \omega_a - \omega_L$ is the detuning between the atomic transition ω_a and the laser frequency ω_L , Ω_0 and g_0 are the maximum Rabi frequencies of the pump field and the maximum single atom-photon cavity-QED coupling strength, respectively. The incoherent part of the cavity field quadrature $\delta \hat{X}_{\mathbf{r}} = \hat{X}_{\mathbf{r}} - \langle \hat{X}_{\mathbf{r}} \rangle$ is instead related to the density fluctuations $\delta \hat{n}_{\mathbf{i}} = \hat{n}_{\mathbf{i}} - \langle \hat{n}_{\mathbf{i}} \rangle$:

$$\langle \delta \hat{X}_{\mathbf{r}} \delta \hat{X}_{\mathbf{r}} \rangle = \frac{\Delta_a^2}{g_0^2 \Omega_0^2} \sum_{\mathbf{i},\mathbf{j}} V_{\mathbf{r},\mathbf{i}} V_{\mathbf{r},\mathbf{j}} \langle \delta \hat{n}_{\mathbf{i}} \delta \hat{n}_{\mathbf{j}} \rangle. \quad (4)$$

The same density correlators are also measurable directly from the incoherent number of photons $\langle \delta \hat{a}_{\mathbf{r}}^\dagger \delta \hat{a}_{\mathbf{r}} \rangle$, but their relation doesn't simply depend on V . We also note that in this adiabatic regime the deviation of the atoms from thermal equilibrium can be neglected for typical experimental timescales [69], and the cavity loss just renormalizes the interaction potential [58].

Figure 3 shows both the coherent and the incoherent component of the cavity field. For the strongly glued droplet regime [Figs. 3(a)–3(e)], we compare the Mott droplet (b),(d) and the SF droplet (c),(e). Since the cavity field resolution is limited by the length scale ξ , the coherent part of the field (b),(c) cannot differentiate these two droplets. They can, however, be distinguished in the incoherent cavity field (d),(e): the SF droplet has higher particle number fluctuations relative to the Mott droplet, hence the higher overall scale of the incoherent field. For the weakly glued droplet regime (Fig. 3(f)–3(j)), we compare the two Mott droplets with $n_c = 1$ (g),(i) and $n_c = 2$ (h),(j). The resolution here is fine enough to distinguish these two droplets using the coherent field (g),(h). Moreover, the incoherent field (i),(j) clearly identifies the droplet edges, where the particle number fluctuations are the highest. The double-peak structure near the edge $i = i_e$ is due to the fact that $\langle (\delta \hat{n}_{i_e})^2 \rangle \approx \langle (\delta \hat{n}_{i_e+1})^2 \rangle \approx -\langle \delta \hat{n}_{i_e} \delta \hat{n}_{i_e+1} \rangle$ across the edge because of the particle number conservation. Since other terms are small, the sum (4) is then maximal at $r - i_e \simeq \pm \xi$, where the derivative of the interaction potential is maximal. The corresponding results for the strongly glued droplet can be understood in a similar fashion: in Fig. 3(d), the two inner peaks of (i) are merged into one due the much larger ξ , while in Fig. 3(e) the SF core plays the same role as the edges for the Mott droplet (particle number fluctuation is indeed highest there), giving rise to two peaks at $r \simeq \pm \xi$.

Outlook.—Other unexplored classes of extended BH models related to the one studied here might be also realized by trapping bosonic mixtures [34,35] or dipolar Bose gases [31,33,37–40] in a lattice. The numerical methods and the analysis employed here offer a helpful guide for the future investigation of new quantum droplet phases in wide class lattice versions of such models. For example, our results can be readily extended to the case of sign-changing interaction, which is naturally realizable in optical cavities and makes possible the existence of density-wave and supersolid droplet phases [58]. In the future, it will be interesting to explore the consequences of the metastability, especially pronounced for weakly glued droplets, for the relaxation dynamics and possible ergodicity breaking or disorder-free localization [47,48].

We thank Tobias Donner, Panos Giannakeas, David Luitz, Alessio Recati, and Maurits Tepaske for helpful discussions. We also thank Francesca Ferlaino and Luis Santos for useful comments on the draft of the paper. P.K. acknowledges the support of the Alexander von Humboldt Foundation, as well the FP7/ERC Consolidator Grant QSIMCORR (No. 771891), the Deutsche Forschungsgemeinschaft (DFG, German Research Foundation) grant under Germany’s Excellence Strategy—EXC-2111—390814868, and the Ministry of Science and Higher Education of the Russian Federation (NUST MISiS Grant No. K2-2020-038).

*karpov@pks.mpg.de

†piazza@pks.mpg.de

- [1] H. Ritsch, P. Domokos, F. Brennecke, and T. Esslinger, Cold atoms in cavity-generated dynamical optical potentials, *Rev. Mod. Phys.* **85**, 553 (2013).
- [2] F. Mivehvar, F. Piazza, T. Donner, and H. Ritsch, Cavity QED with quantum gases: new paradigms in many-body physics, *Adv. Phys.* **70**, 1 (2021).
- [3] J. Klinder, H. Keßler, M. R. Bakhtiari, M. Thorwart, and A. Hemmerich, Observation of a Superradiant Mott Insulator in the Dicke-Hubbard Model, *Phys. Rev. Lett.* **115**, 230403 (2015).
- [4] R. Landig, L. Hruby, N. Dogra, M. Landini, R. Mottl, T. Donner, and T. Esslinger, Quantum phases from competing short- and long-range interactions in an optical lattice, *Nature (London)* **532**, 476 (2016).
- [5] Y. Li, L. He, and W. Hofstetter, Lattice-supersolid phase of strongly correlated bosons in an optical cavity, *Phys. Rev. A* **87**, 051604(R) (2013).
- [6] M. R. Bakhtiari, A. Hemmerich, H. Ritsch, and M. Thorwart, Nonequilibrium Phase Transition of Interacting Bosons in an Intra-Cavity Optical Lattice, *Phys. Rev. Lett.* **114**, 123601 (2015).
- [7] N. Dogra, F. Brennecke, S. D. Huber, and T. Donner, Phase transitions in a Bose-Hubbard model with cavitymediated global-range interactions, *Phys. Rev. A* **94**, 023632 (2016).
- [8] Y. Chen, Z. Yu, and H. Zhai, Quantum phase transitions of the Bose-Hubbard model inside a cavity, *Phys. Rev. A* **93**, 041601(R) (2016).
- [9] B. Sundar and E. J. Mueller, Lattice bosons with inniterange checkerboard interactions, *Phys. Rev. A* **94**, 033631 (2016).
- [10] T. Flottat, L. deForges de Parny, F. Hébert, V. G. Rousseau, and G. G. Batrouni, Phase diagram of bosons in a two-dimensional optical lattice with innite-range cavitymediated interaction, *Phys. Rev. B* **95**, 144501 (2017).
- [11] J. Panas, A. Kauch, and K. Byczuk, Phase diagram of bosons in a two-dimensional optical lattice with innite-range cavitymediated interactio, *Phys. Rev. B* **95**, 115105 (2017).
- [12] E. I. Rodríguez Chiacchio and A. Nunnenkamp, Tuning the relaxation dynamics of ultracold atoms in a lattice with an optical cavity, *Phys. Rev. A* **97**, 033618 (2018).
- [13] D. Nagy, G. Kónya, P. Domokos, and G. Szirmai, Quantum noise in a transversely-pumped-cavity Bose-Hubbard model, *Phys. Rev. A* **97**, 063602 (2018).
- [14] R. Liao, H.-J. Chen, D.-C. Zheng, and Z.-G. Huang, Theoretical exploration of competing phases of lattice Bose gases in a cavity, *Phys. Rev. A* **97**, 013624 (2018).
- [15] L. Himbert, C. Cormick, R. Kraus, S. Sharma, and G. Morigi, Mean-eld phase diagram of the extended Bose-Hubbard model of many-body cavity quantum electrodynamics, *Phys. Rev. A* **99**, 043633 (2019).
- [16] J. Léonard, A. Morales, P. Zupancic, T. Esslinger, and T. Donner, Mean-eld phase diagram of the extended Bose-Hubbard model of many-body cavity quantum electrodynamics, *Nature (London)* **543**, 87 (2017).
- [17] J. Lang, F. Piazza, and W. Zwerger, Collective excitations and supersolid behavior of bosonic atoms inside two crossed optical cavities, *New J. Phys.* **19**, 123027 (2017).
- [18] F. Mivehvar, S. Ostermann, F. Piazza, and H. Ritsch, Driven-dissipative supersolid in a ring cavity, *Phys. Rev. Lett.* **120**, 123601 (2018).
- [19] S. C. Schuster, P. Wolf, S. Ostermann, S. Slama, and C. Zimmermann, Supersolid Properties of a Bose- Einstein Condensate in a Ring Resonator, *Phys. Rev. Lett.* **124**, 143602 (2020).
- [20] A. J. Kollár, A. T. Papageorge, K. Baumann, M. A. Armen, and B. L. Lev, An adjustable-length cavity and Bose-Einstein condensate apparatus for multimode cavity QED, *New J. Phys.* **17**, 043012 (2015).
- [21] A. J. Kollár, A. T. Papageorge, V. D. Vaidya, Y. Guo, J. Keeling, and B. L. Lev, Supermode-density-wavepolariton condensation with a Bose-Einstein condensate in a multimode cavity, *Nat. Commun.* **8**, 14386 (2017).
- [22] V. D. Vaidya, Y. Guo, R. M. Kroeze, K. E. Ballantine, A. J. Kollár, J. Keeling, and B. L. Lev, Tunable- Range, Photon-Mediated Atomic Interactions in Multimode Cavity QED, *Phys. Rev. X* **8**, 011002 (2018).
- [23] Y. Guo, R. M. Kroeze, V. D. Vaidya, J. Keeling, and B. L. Lev, Sign-Changing Photon-Mediated Atom Interactions in Multimode Cavity Quantum Electrodynamics, *Phys. Rev. Lett.* **122**, 193601 (2019).
- [24] Y. Guo, R. M. Kroeze, B. P. Marsh, S. Gopalakrishnan, J. Keeling, and B. L. Lev, An optical lattice with sound, *Nature (London)* **599**, 211 (2021).
- [25] S. Gopalakrishnan, B. L. Lev, and P. M. Goldbart, Emergent crystallinity and frustration with Bose-Einstein condensates in multimode cavities, *Nat. Phys.* **5**, 845 (2009).
- [26] S. Gopalakrishnan, B. L. Lev, and P. M. Goldbart, Atomlight crystallization of Bose-Einstein condensates in

- multimode cavities: Nonequilibrium classical and quantum phase transitions, emergent lattices, supersolidity, and frustration, *Phys. Rev. A* **82**, 043612 (2010).
- [27] P. Karpov and F. Piazza, Crystalline droplets with emergent color charge in many-body systems with signchanging interactions, *Phys. Rev. A* **100**, 061401(R) (2019).
- [28] S. M. A. Rombouts, K. Van Houcke, and L. Pollet, Loop Updates for Quantum Monte Carlo Simulations in the Canonical Ensemble, *Phys. Rev. Lett.* **96**, 180603 (2006).
- [29] K. Van Houcke, S. M. A. Rombouts, and L. Pollet, Loop Updates for Quantum Monte Carlo Simulations in the Canonical Ensemble, *Phys. Rev. E* **73**, 056703 (2006).
- [30] L. Pollet, Ultracold atoms in an optical lattice: A numerical approach, Ph.D. thesis, Ghent University, 2005, <http://compphys.ugent.be/docs/phd/LodePollet.pdf>.
- [31] M. Schmitt, M. Wenzel, F. Böttcher, I. Ferrier-Barbut, and T. Pfau, Self-bound droplets of a dilute magnetic quantum liquid, *Nature (London)* **539**, 259 (2016).
- [32] I. Ferrier-Barbut, H. Kadau, M. Schmitt, M. Wenzel, and T. Pfau, Observation of quantum droplets in a strongly dipolar bose gas, *Phys. Rev. Lett.* **116**, 215301 (2016).
- [33] L. Chomaz, S. Baier, D. Petter, M. J. Mark, F. Wächtler, L. Santos, and F. Ferlaino, Quantum-Fluctuation-Driven Crossover from a Dilute Bose-Einstein Condensate to a Macrodroplet in a Dipolar Quantum Fluid, *Phys. Rev. X* **6**, 041039 (2016).
- [34] C. R. Cabrera, L. Tanzi, J. Sanz, B. Naylor, P. Thomas, P. Cheiney, and L. Tarruell, Quantum liquid droplets in a mixture of Bose-Einstein condensates, *Science* **359**, 301 (2018).
- [35] G. Semeghini, G. Ferioli, L. Masi, C. Mazzinghi, L. Wolswijk, F. Minardi, M. Modugno, G. Modugno, M. Inguscio, and M. Fattori, Self-Bound Quantum Droplets of Atomic Mixtures in Free Space, *Phys. Rev. Lett.* **120**, 235301 (2018).
- [36] F. Böttcher, J.-N. Schmidt, J. Hertkorn, K. S. Ng, S. D. Graham, M. Guo, T. Langen, and T. Pfau, New states of matter with ne-tuned interactions: quantum droplets and dipolar supersolids, *Rep. Prog. Phys.* **84**, 012403 (2021).
- [37] L. Pollet, Quantum gases show ashes of a supersolid, *Nature (London)* **569**, 494 (2019).
- [38] L. Tanzi, E. Lucioni, F. Famà, J. Catani, A. Fioretti, C. Gabbanini, R. N. Bisset, L. Santos, and G. Modugno, Observation of a Dipolar Quantum Gas with Metastable Supersolid Properties, *Phys. Rev. Lett.* **122**, 130405 (2019).
- [39] F. Böttcher, J.-N. Schmidt, M. Wenzel, J. Hertkorn, M. Guo, T. Langen, and T. Pfau, Transient Supersolid Properties in An Array of Dipolar Quantum Droplets, *Phys. Rev. X* **9**, 011051 (2019).
- [40] L. Chomaz, D. Petter, P. Ilzhöfer, G. Natale, A. Trautmann, C. Politi, G. Durastante, R. M. W. van Bijnen, A. Patscheider, M. Sohmen, M. J. Mark, and F. Ferlaino, Long-Lived and Transient Supersolid Behaviors in Dipolar Quantum Gases, *Phys. Rev. X* **9**, 021012 (2019).
- [41] Y. Kora and M. Boninsegni, Patterned supersolids in dipolar bose systems, *J. Low Temp. Phys.* **197**, 337 (2019).
- [42] J. Hertkorn, J.-N. Schmidt, M. Guo, F. Böttcher, K. Ng, S. Graham, P. Uerlings, T. Langen, M. Zwierlein, and T. Pfau, Pattern formation in quantum ferrofluids: From supersolids to superglasses, *Phys. Rev. Research* **3**, 033125 (2021).
- [43] Y.-C. Zhang, T. Pohl, and F. Maucher, Phases of supersolids in conned dipolar Bose-Einstein condensates, *Phys. Rev. A* **104**, 013310 (2021).
- [44] M. A. Norcia, C. Politi, L. Klaus, E. Poli, M. Sohmen, M. J. Mark, R. N. Bisset, L. Santos, and F. Ferlaino, Two-dimensional supersolidity in a dipolar quantum gas, *Nature (London)* **596**, 357 (2021).
- [45] K. Góral, L. Santos, and M. Lewenstein, Quantum Phases of Dipolar Bosons in Optical Lattices, *Phys. Rev. Lett.* **88**, 170406 (2002).
- [46] S. Baier, M. J. Mark, D. Petter, K. Aikawa, L. Chomaz, Z. Cai, M. Baranov, P. Zoller, and F. Ferlaino, Extended Bose-Hubbard models with ultracold magnetic atoms, *Science* **352**, 201 (2016).
- [47] W. Li, A. Dhar, X. Deng, K. Kasamatsu, L. Barbiero, and L. Santos, Disorderless Quasi-Localization of Polar Gases in One-Dimensional Lattices, *Phys. Rev. Lett.* **124**, 010404 (2020).
- [48] W.-H. Li, X. Deng, and L. Santos, Hilbert Space Shattering and Disorder-Free Localization in Polar Lattice Gases,, *Phys. Rev. Lett.* **127**, 260601 (2021).
- [49] I. Morera, G. E. Astrakharchik, A. Polls, and B. Juliá-Díaz, Quantum droplets of bosonic mixtures in a onedimensional optical lattice, *Phys. Rev. Research* **2**, 022008(R) (2020).
- [50] I. Morera, G. E. Astrakharchik, A. Polls, and B. Juliá-Díaz, Universal Dimerized Quantum Droplets in a One-dimensional Lattice, *Phys. Rev. Lett.* **126**, 023001 (2021).
- [51] O. Dutta, M. Gajda, P. Hauke, M. Lewenstein, D.-S. Lühmann, B. A. Malomed, T. Sowiński, and J. Zakrzewski, Non-standard Hubbard models in optical lattices: A review, *Rep. Prog. Phys.* **78**, 066001 (2015).
- [52] S. Ostermann, F. Piazza, and H. Ritsch, Non-Standard Hubbard Models in Optical Lattices: A Review, *Phys. Rev. X* **6**, 021026 (2016).
- [53] G. Labeyrie, E. Tesio, P. M. Gomes, G. L. Oppo, W. J. Firth, G. R. M. Robb, A. S. Arnold, R. Kaiser, and T. Ackemann, Optomechanical self-structuring in a cold atomic gas, *Nat. Photonics* **8**, 321 (2014).
- [54] E. Tesio, G. R. M. Robb, T. Ackemann, W. J. Firth, and G.-L. Oppo, Kinetic Theory for Transverse Optomechanical Instabilities, *Phys. Rev. Lett.* **112**, 043901 (2014).
- [55] G. R. M. Robb, E. Tesio, G.-L. Oppo, W. J. Firth, T. Ackemann, and R. Bonifacio, Quantum Threshold for Optomechanical Self-Structuring in a Bose-Einstein Condensate, *Phys. Rev. Lett.* **114**, 173903 (2015).
- [56] Y.-C. Zhang, V. Walther, and T. Pohl, Long-Range Interactions and Symmetry Breaking in Quantum Gases through Optical Feedback, *Phys. Rev. Lett.* **121**, 073604 (2018).
- [57] Y.-C. Zhang, V. Walther, and T. Pohl, Self-bound droplet clusters in laser-driven Bose-Einstein condensates, *Phys. Rev. A* **103**, 023308 (2021).
- [58] See Supplemental Material at <http://link.aps.org/supplemental/10.1103/PhysRevLett.128.103201> for the derivation of the extended Bose-Hubbard model, details about the droplet profile in the Thomas-Fermi limit, the results on the finite-size effects and benchmarks versus exact diagonalization for the droplets in 1D, and the results on the droplets in 2D with sign-changing interaction.

-
- [59] C. H. Johansen, J. Lang, A. Morales, A. Baumgärtner, T. Donner, and F. Piazza, Multimode-polariton superradiance via Floquet engineering, [arXiv:2011.12309](https://arxiv.org/abs/2011.12309).
- [60] V. Torggler and H. Ritsch, Adaptive multifrequency light collection by self-ordered mobile scatterers in optical resonators, *Optica* **1**, 336 (2014).
- [61] Y. Guo, V. D. Vaidya, R. M. Kroeze, R. A. Lunney, B. L. Lev, and J. Keeling, Emergent and broken symmetries of atomic self-organization arising from Gouy phase shifts in multimode cavity QED, *Phys. Rev. A* **99**, 053818 (2019).
- [62] N. Prokofev, B. Svistunov, and I. Tupitsyn, , *J. Exp. Theor. Phys.* **87**, 310 (1998).
- [63] A. W. Sandvik, Stochastic series expansion method with operator-loop update, *Phys. Rev. B* **59**, R14157 (1999).
- [64] O. F. Syljuåsen and A. W. Sandvik, Quantum monte carlo with directed loops, *Phys. Rev. E* **66**, 046701 (2002).
- [65] U. Schollwöck, The density-matrix renormalization group, *Rev. Mod. Phys.* **77**, 259 (2005).
- [66] D. van Oosten, P. van der Straten, and H. T. C. Stoof, Quantum phases in an optical lattice, *Phys. Rev. A* **63**, 053601 (2001).
- [67] R. Kanamoto, H. Saito, and M. Ueda, Quantum phase transition in one-dimensional Bose-Einstein condensates with attractive interactions, *Phys. Rev. A* **67**, 013608 (2003).
- [68] M. P. A. Fisher, P. B. Weichman, G. Grinstein, and D. S. Fisher, Boson localization and the superfluid-insulator transition, *Phys. Rev. B* **40**, 546 (1989).
- [69] See discussion in Sec. 2.6 of [2].